Electronic Supplementary Material (ESI) for Physical Chemistry Chemical Physics.

Electronic Supporting Information for: Structural Dynamics of an Excited Donor-Acceptor Complex from Ultrafast Polarized Infrared Spectroscopy, Molecular Dynamics Simulations, and Quantum Chemical Calculations

Christopher A. Rumble*, Eric Vauthey*
Department of Physical Chemistry
University of Geneva
30 Quai Ernest-Ansermet, CH-1211 Geneva 4, Switzerland

*Email: christopher.rumble@unige.ch, eric.vauthey@unige.ch

All data are available for download at:
http://doi.org/10.5281/zenodo.2872150.

Contents

List of Figures

List of Tables

S1 Transient Visible Absorption

Samples were excited at 400 nm by frequency doubling part of the 800 nm fundamental of a 1 kHz Ti:Sapphire amplified laser system (Spectra Physics Spitfire) and white light probe pulses were generated using another part of the 800 nm fundamental and a 3 mm CaF_2 plate. The pump beam was polarized at magic angle relative to the probe and overlapped at the sample which was contained in a 1 mm quartz flow cell. Samples were not recirculated due to the accumulation of dark colored photoproducts. Simultaneous detection of the signal and reference spectra was achieved using a pair of spectrographs (Andor Technology, SR163) and CCD cameras (Hamamatsu S07030-09).

After the data were collected, a wavelength dependent time-zero correction was applied using a Kerr effect measurement in CH_2Cl_2,(1) and a holmium filter measurement was used for wavelength calibration of the spectrograph. Spontaneous emission was removed using a background subtraction procedure. Measurements were performed from -20 to 200 ps and truncated to 0.5 to 200 ps after processing to avoid short time coherent artifacts and broadening from the instrument function. No instrument function deconvolution was performed. The temporal resolution of the instrument is wavelength dependent and estimated to be 100-350 fs. Global analysis(2) was performed on the truncated data set using an in-house procedure implemented in MATLAB R2017A.

S2 Transient Infrared Absorption

Excitation was at 400 nm and generated by frequency doubling part of the 800 nm fundamental of a 1 kHz Ti:Sapphire amplified laser system (Spectra Physics Solstice). Another part of the fundamental was then used to generate mid-IR probe pulses by difference frequency generation using the output of an optical parametric amplifier (Light Conversion TOPAS-C with NDFG attachment). The probe beam was polarized vertically using a wire grid polarizer and the pump was polarized using a Glan-Laser polarizer oriented either parallel, perpendicular, or at magic angle with respect to the probe. Signal and reference mid-IR beams were focused into an imaging spectrograph (Horiba, Triax 190) and detected using a MCT detector with 2 rows of 64 detection elements cooled with liquid nitrogen. The wavelength resolution of the detection system was $\sim$3 cm^{-1}, and the temporal resolution was estimated to be $\sim$300 fs. Samples were contained in a flow cell consisting of two CaF_2 windows separated by a 0.3 mm spacer.(3)

TRIR spectra were collected from -20 to 200 ps by collecting 2000 laser shots per time step in the C$\equiv$N stretch region, $\sim$2100–2310 cm^{-1}. This process was repeated 8 times for magical angle, parallel, and perpendicular polarizer orientations (alternating polarization between each scan) for a total of 24 scans. These data were then background subtracted, averaged, and truncated to 0.5 to 200 ps to avoid short-time coherent effects. The magic angle data were fit using the same global analysis procedure as the visTA data.

TRIR anisotropies were determined by simultaneously fitting single wavenumber TRIR traces under parallel, perpendicular, and magic angle polarizer conditions. The magic angle trace, $\Delta A(t)$, was fit with a sum of three exponentials,

$$\Delta A(t) = bkg + h\sum_{i=1}^{3} a_i \exp(-t/\tau_i), \tag{1}$$

where bkg a background offset and h is a scaling factor. The polarized traces, $\Delta A_{\|}(t)$ and $\Delta A_{\perp}(t)$, were fit with

$$\begin{aligned} \Delta A_{\|}(t) &\propto \Delta A(t)[1 - r(t)] \\ \Delta A_{\perp}(t) &\propto G\Delta A(t)[1 + 2r(t)], \end{aligned} \tag{2}$$

where G is a fitted instrumental polarization sensitivity correction factor. The anisotropy, $r(t)$, was described using one or two exponentials:

$$r(t) = \sum_i r_i \exp(-t/\tau_{r,i}), \quad i = 1 \text{ or } 2. \tag{3}$$

The initial anisotropy, r_0, was determined by $r_0 = \sum_i r_i$. Residuals of all three traces were minimized simultaneously using a non-linear least squares routine implemented in MATLAB R2017A.

S3 Molecular Dynamics Methods

All MD simulations were performed using the GROMACS 2018.1 package,(4) and the OPLS-AA force field.(5) Integration was carried out using the Verlet leap-frog algorithm with a step size of 2 fs. Non-bonded interactions were calculated using a Verlet neighbor list with a cutoff radius of 1.4 nm. Long-range electrostatics were handled using the particle-mesh Ewald method.(6) Hydrogen-containing bonds were constrained using the P-LINCS algorithm.(7) Temperature was set to 293.15 K and was controlled using the modified Berendsen thermostat with a relaxation time of 0.5 ps.(8) Scripting of the simulations and TD-DFT calculations was accomplished using Python 3.6, and coordinates from the simulations were extracted using the MDAnalysis package.(9,10) All other calculations and analyses were performed using in-house procedures implemented in Python 3.6 or MATLAB R2017A.

To build and equilibrate the initial simulation box, Bz and TCNE solutes were placed opposite from each other at a distance of 1 nm from the center of 8×8×8 nm simulation box with cubic periodic boundary conditions. The box was then packed with 4600 CH_2Cl_2 molecules using the GROMACS *insert-molecules* module. An energy minimization procedure was carried out using the steepest-descent method with a maximum force stopping point of 500 kJ mol^{-1} nm^{-1}. Next, three consecutive 500 ps simulations were performed in the NVT, NPT, and NVT ensembles. The pressure in the NPT simulation was set to 1.013 bar and regulated using the Berendsen barostat with a relaxation time of 5 ps. The system was then propagated for a time sufficient to generate a configuration with a Bz/TCNE center-of-mass distance (r) less than 0.35 nm. This configuration was selected for the beginning of the pull simulation.

A pull simulation was then performed by fixing Bz to the center of the box using a harmonic potential with a 1000 kJ mol^{-1} nm^{-2} spring constant and pulling the TCNE molecule at a rate of 0.01 nm ps^{-1}, also using a harmonic potential with a spring constant of 1000 kJ mol^{-1} nm^{-2}. From this simulation, 50 configurations were selected with center-of-mass separations of 0.35 nm $< r <$ 3.5 nm as starting points for the umbrella sampling simulations. Umbrella sampling was then carried out on these 50 configurations by fixing Bz and TCNE positions with 1000 kJ mol^{-1} nm^{-2} harmonic potentials and simulating for 15.5 ns with the first 0.5 ns discarded as equilibration. Energies were saved every 1 ps, and the weighted histogram analysis method (WHAM) was used to calculate the Bz/TCNE potential of mean force, $w(r)$, using the GROMACS *wham* module.(11) The umbrella sampling simulations were then repeated using Bz$^{\cdot+}$/TCNE$^{\cdot-}$charges in order to calculate $w(r)$ for the ionic pair.

S4 Conformation Selection Procedure

In order to select a representative set of Bz/TCNE conformations for the TD-DFT and non-equilibrium MD simulations, we begin by partitioning the space between 0.31 and 0.97 nm into 40 linearly spaced bins and assign each structure generated by the PMF calculation to one of these bins. A weight for each bin is then calculated according to:

$$n_i = \int_{r_{i,\text{low}}}^{r_{i\text{high}}} r^2 g(r) dr \tag{4}$$

where n_i is the weight assigned to bin i, $r_{i,\text{low}}$ and $r_{i,\text{high}}$ are the low and high bin edges, and $g(r)$ is the pair distribution function calculated using the simulated potential of mean force by $g(r) = \exp[-w(r)/k_B T]$. The weights are then normalized to the sum of all bin weights and multiplied by 1500 to determine the number of conformations to randomly select from each bin (rounding up for fractions). In this fashion, 1505 Bz/TCNE conformations were selected for the TD-DFT calculations and non-equilibrium MD simulations.

S5 Anisotropy Calculation from Non-Equilibrium MD Simualtions

From each of the 1505 non-equilibrium trajectories, anisotropies were calculated according to Equation 1 of the main text using the transition dipoles from the TD-DFT calculations as $\hat{M}_\text{ex}$, and $\hat{M}_1(t)$ and $\hat{M}_2(t)$ taken from the TCNE coordinates at each time step of the non-equilibrium MD simulation. The final simulated anisotropy was then calculated by averaging the 1505 individual correlation functions weighted by their oscillator strengths according to:

$$r_\text{sim}^{(i)}(t) = \frac{1}{f_\text{tot}} \sum_{j=1}^{2} \sum_{k=1}^{n_\text{sim}} f_{j,k} r_{j,k}^{(i)}(t) \tag{5}$$

where $i = 1, 2$ indicates TCNE vibrational transition dipole $\hat{M}_1$ or $\hat{M}_2$, $j = 1, 2$ indicates CT transition 1 or 2, k indicates one of the $n_{\text{sim}} = 1505$ non-equilibrium trajectories, $f_{j,k}$ is the oscillator strength for CT transition j for trajectory k, $f_{\text{tot}} = \sum_j \sum_k f_{j,k}$ is the sum of all oscillator strengths, and $r_{j,k}^{(i)}(t)$ is the anisotropy of TCNE vibration i, CT transition j, and simulation index k. This calculation is analogous to exciting the entire absorption spectrum and watching the anisotropy evolve.

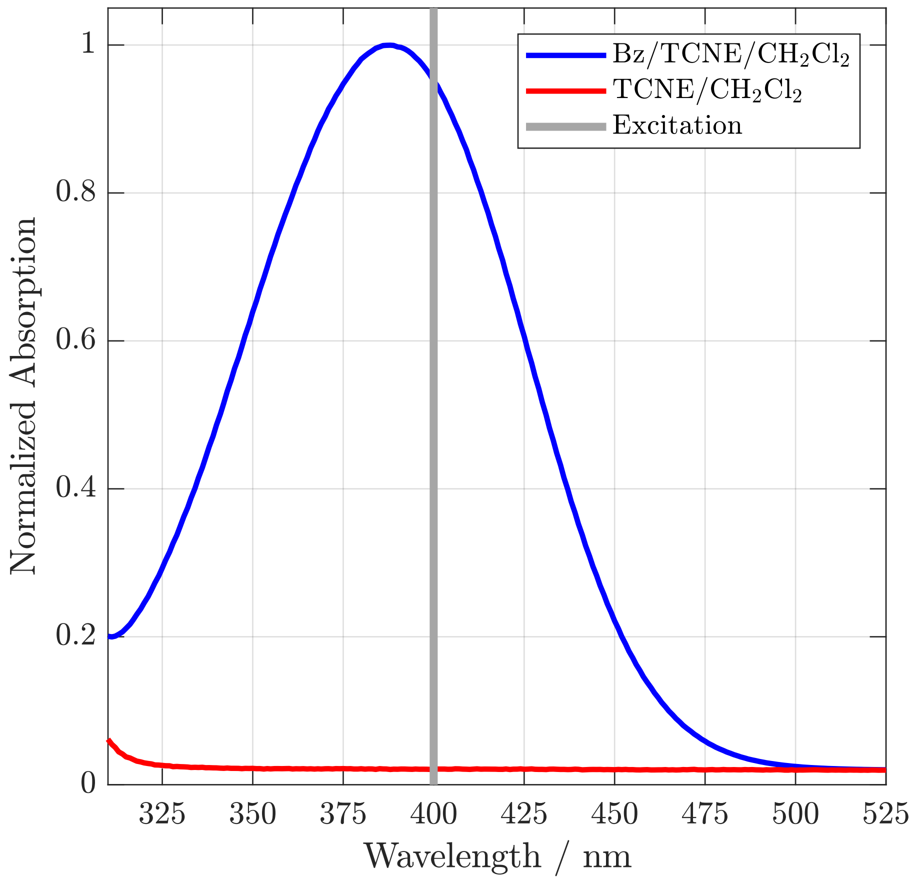

Figure S1: Steady-state UV-vis absorption spectra of Bz/TCNE/CH_2Cl_2 and TCNE/CH_2Cl_2 with the 400 nm excitation wavelength of the visTA and TRIR experiments labeled.

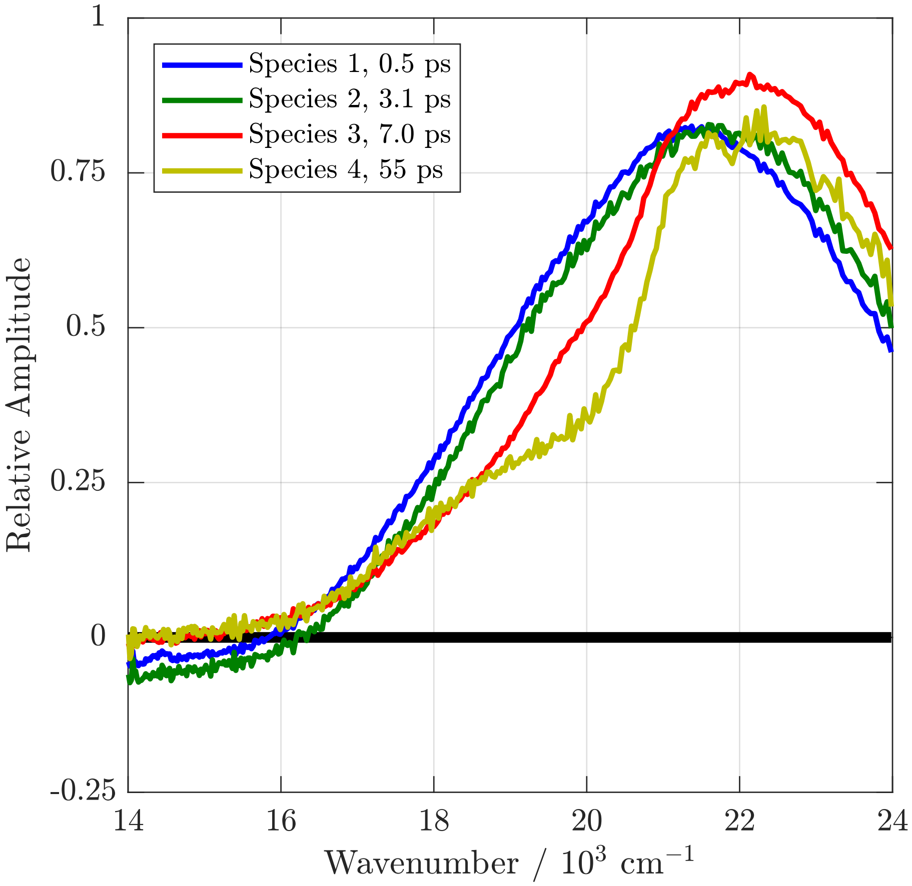

Figure S2: Evolution associated difference spectra (EADS) from global analysis of the Bz/TCNE/CH_2Cl_2 visTA data.

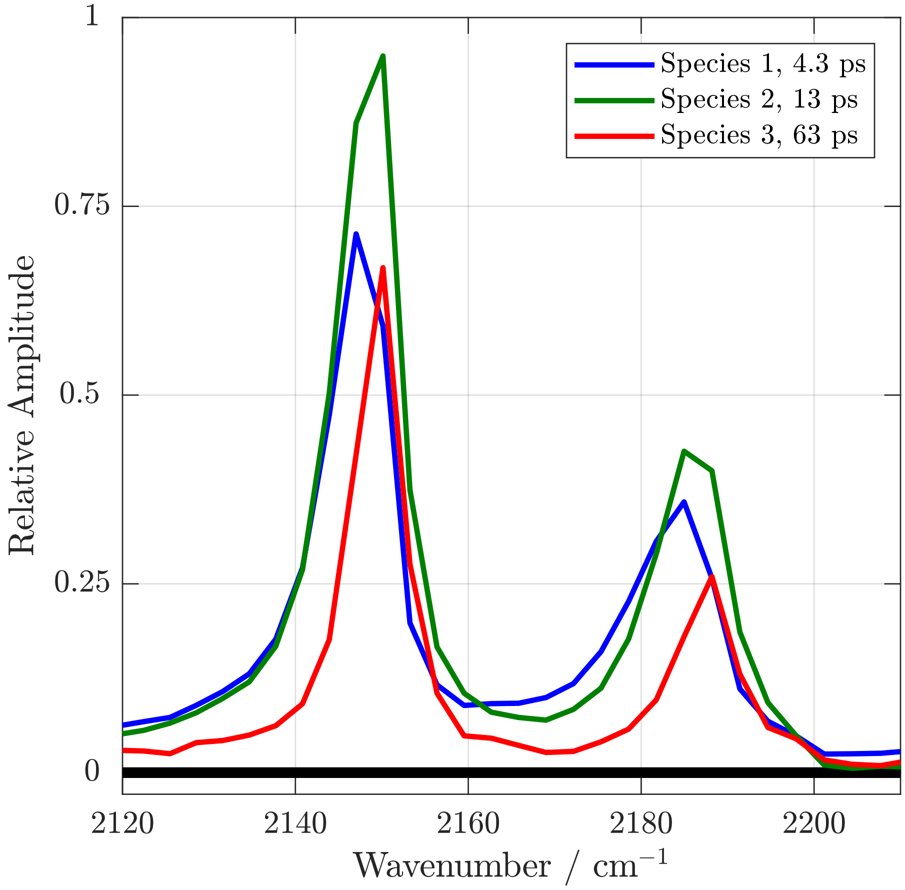

Figure S3: Evolution associated difference spectra (EADS) from global analysis of the Bz/TCNE/CH_2Cl_2 TRIR data.

Table S1: Benzene/TCNE/CH_2Cl_2 TRIR anisotropy fitting parameters. Parameter definitions are given in Section 2.2 of the main text. Uncertainties of 10-30% in these parameters are estimated based on the standard deviation of replicate measurements. The largest uncertainty is found in the slow anisotropy time constant $\tau_{r,2}$, as it is on the order of the slowest population time constant, τ_3.

Population Parameters

$\tilde{\nu}$	h	bkg	a_1	τ_1 / ps	a_2	τ_2 / ps	a_3	τ_3 / ps
2141	4.02	0.01	-0.38	9.4	0.52	12	0.10	65
2144	4.64	0.00	-0.32	8.3	0.52	14	0.16	68
2147	4.77	0.04	-0.25	4.9	0.26	15	0.50	50
2150	5.94	0.04	-0.13	1.7	-0.22	9.3	0.65	52
2182	4.93	-0.02	-0.39	8.3	0.52	10	0.10	70
2185	2.30	-0.02	-0.23	3.9	0.28	12	0.49	52
2188	2.29	0.02	-0.14	2.1	-0.18	8.6	0.68	51

Anisotropy Parameters

$\tilde{\nu}$	G	r_0	r_1	$\tau_{r,1}$ / ps	r_2	$\tau_{r,2}$ / ps
2141	0.996	-0.08	-0.12	5.5	0.04	64
2144	0.993	-0.10	-0.14	5.5	0.04	47
2147	0.976	-0.10	-0.16	5.9	0.06	47
2150	0.998	-0.08	-0.15	5.9	0.07	60
2182	0.943	-0.05	-0.05	2.9	–	–
2185	0.981	-0.07	-0.07	4.8	–	–
2188	0.979	-0.06	-0.06	9.8	–	–

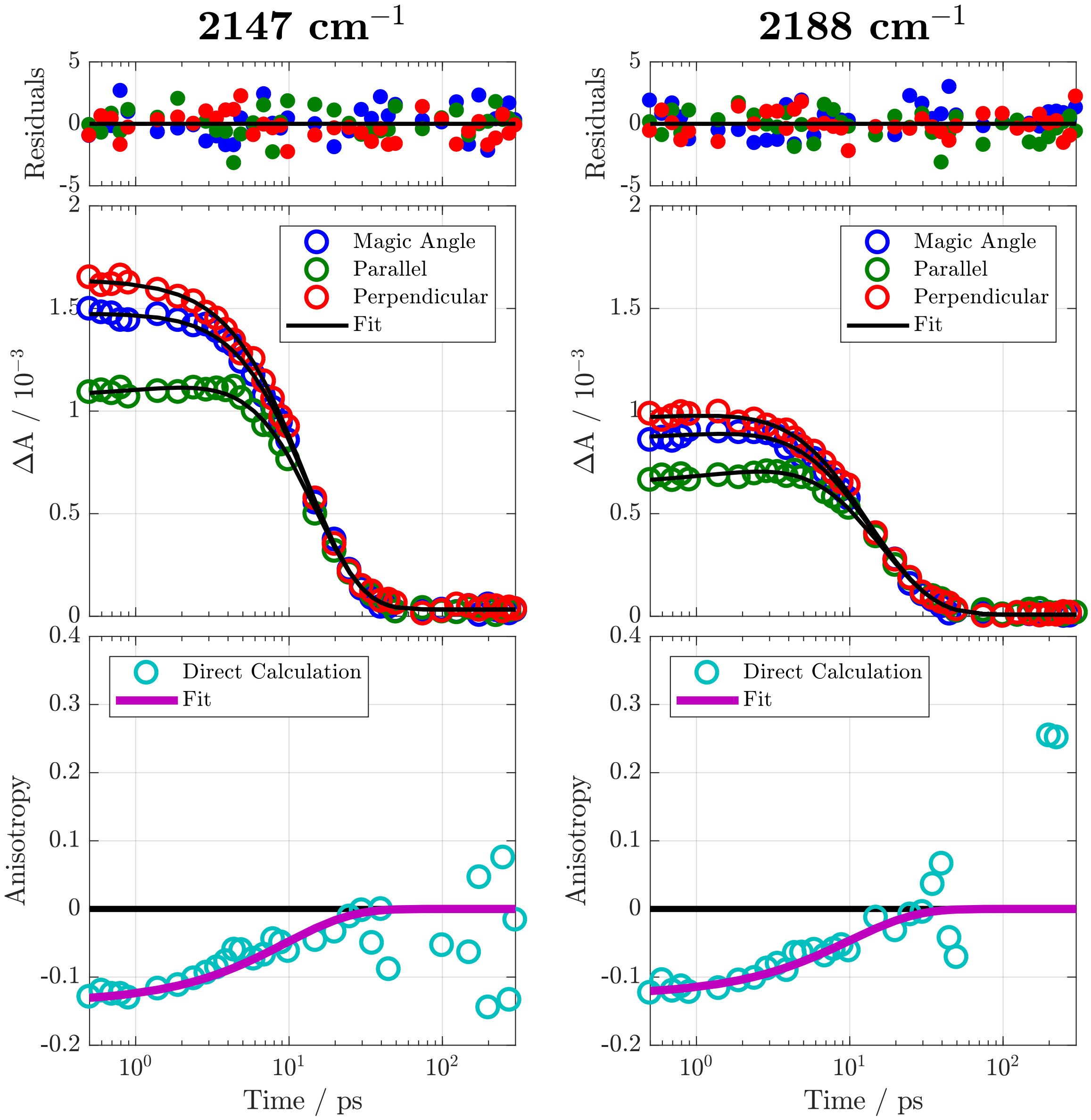

Figure S4: Representative toluene/TCNE/CH_2Cl_2 TRIR and anisotropy traces.

Table S2: Toluene/TCNE/CH_2Cl_2 TRIR anisotropy fitting parameters. Parameter definitions are given in Section 2.2 of the main text.

Population Parameters

$\tilde{\nu}$	h	bkg	a_1	τ_1 / ps	a_2	τ_2 / ps	a_3	τ_3 / ps
2141	1.25	0.02	-0.28	2.9	0.72	9	–	–
2144	3.24	0.03	-0.36	4.3	0.64	7	–	–
2147	5.33	0.03	-0.37	4.9	0.63	9	–	–
2150	4.20	0.03	-0.29	3.0	0.71	12	–	–
2182	1.42	0.01	-0.30	4.7	0.70	9	–	–
2185	2.24	0.03	-0.32	4.6	0.68	9	–	–
2188	1.77	0.01	-0.26	3.0	0.74	12	–	–

Anisotropy Parameters

$\tilde{\nu}$	G	r_0	r_1	$\tau_{r,1}$ / ps	r_2	$\tau_{r,2}$ / ps
2141	0.895	-0.15	-0.15	10.6	–	–
2144	0.973	-0.13	-0.13	11.3	–	–
2147	0.980	-0.14	-0.14	9.4	–	–
2150	0.969	-0.14	-0.14	9.1	–	–
2182	0.949	-0.13	-0.13	19.0	–	–
2185	0.976	-0.13	-0.13	10.0	–	–
2188	0.989	-0.13	-0.13	9.9	–	–

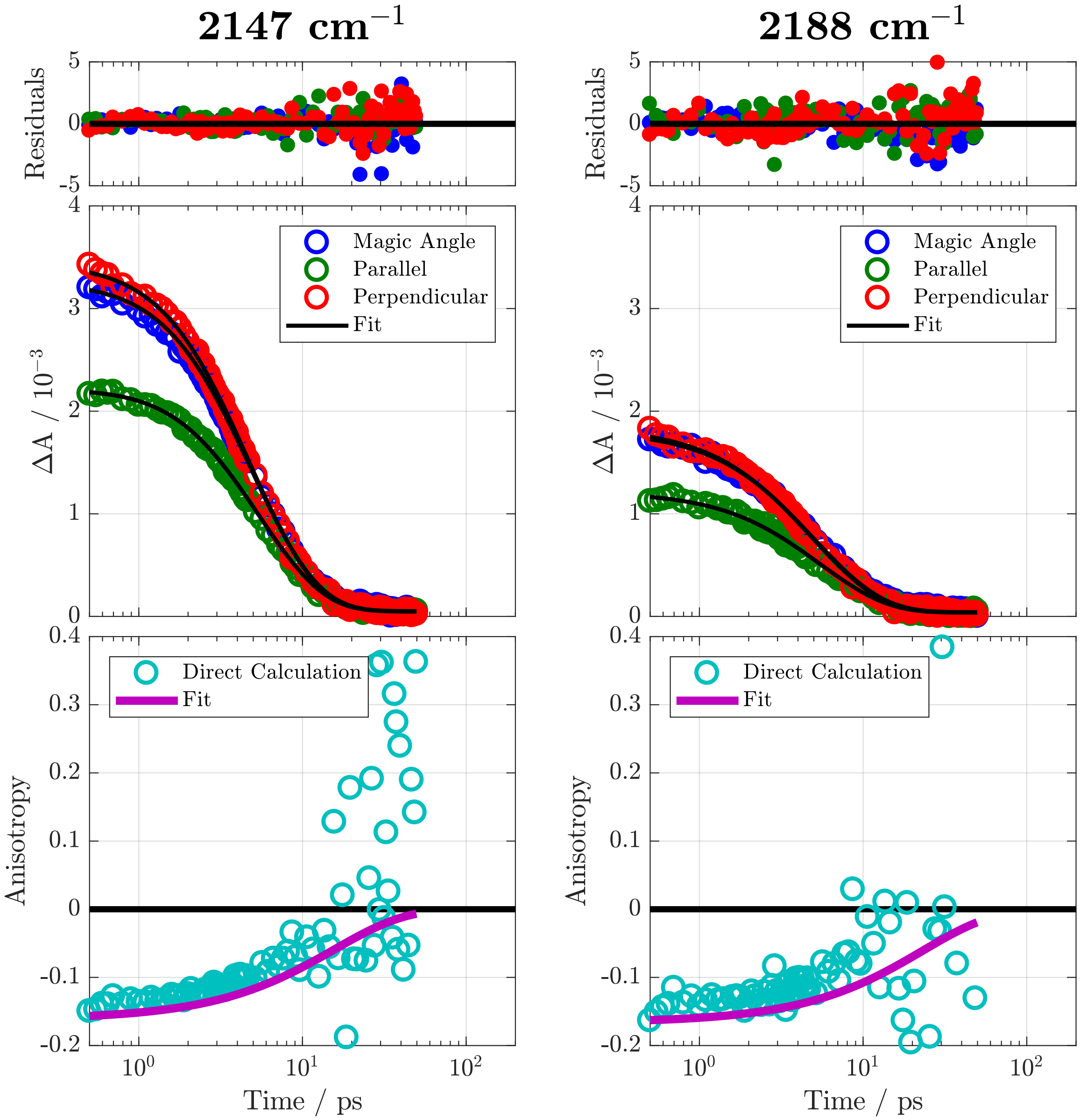

Figure S5: Representative *p*-xylene/TCNE/CH_2Cl_2 TRIR and anisotropy traces.

Table S3: *p*-xylene/TCNE/CH_2Cl_2 TRIR anisotropy fitting parameters. Parameter definitions are given in Section 2.2 of the main text.

Population Parameters

$\tilde{\nu}$	h	bkg	a_1	τ_1 / ps	a_2	τ_2 / ps	a_3	τ_3 / ps
2141	2.70	0.04	-0.19	1.3	0.81	4.0	–	–
2144	3.83	0.05	-0.16	1.0	0.84	4.0	–	–
2147	4.99	0.05	-0.18	1.0	0.82	5.0	–	–
2150	4.37	0.05	-0.25	1.0	0.75	5.0	–	–
2182	1.66	0.02	1.00	5.0	–	5.0	–	–
2185	2.28	0.04	-0.11	0.9	0.89	5.0	–	–
2188	1.70	0.06	-0.20	0.9	0.80	5.0	–	–

Anisotropy Parameters

$\tilde{\nu}$	G	r_0	r_1	$\tau_{r,1}$ / ps	r_2	$\tau_{r,2}$ / ps
2141	0.955	-0.14	-0.14	26.5	–	–
2144	0.937	-0.15	-0.15	19.2	–	–
2147	0.911	-0.16	-0.16	15.6	–	–
2150	0.865	-0.17	-0.17	15.9	–	–
2182	0.904	-0.16	-0.16	50.0	–	–
2185	0.872	-0.17	-0.17	23.0	–	–
2188	0.911	-0.16	-0.16	50.0	–	–

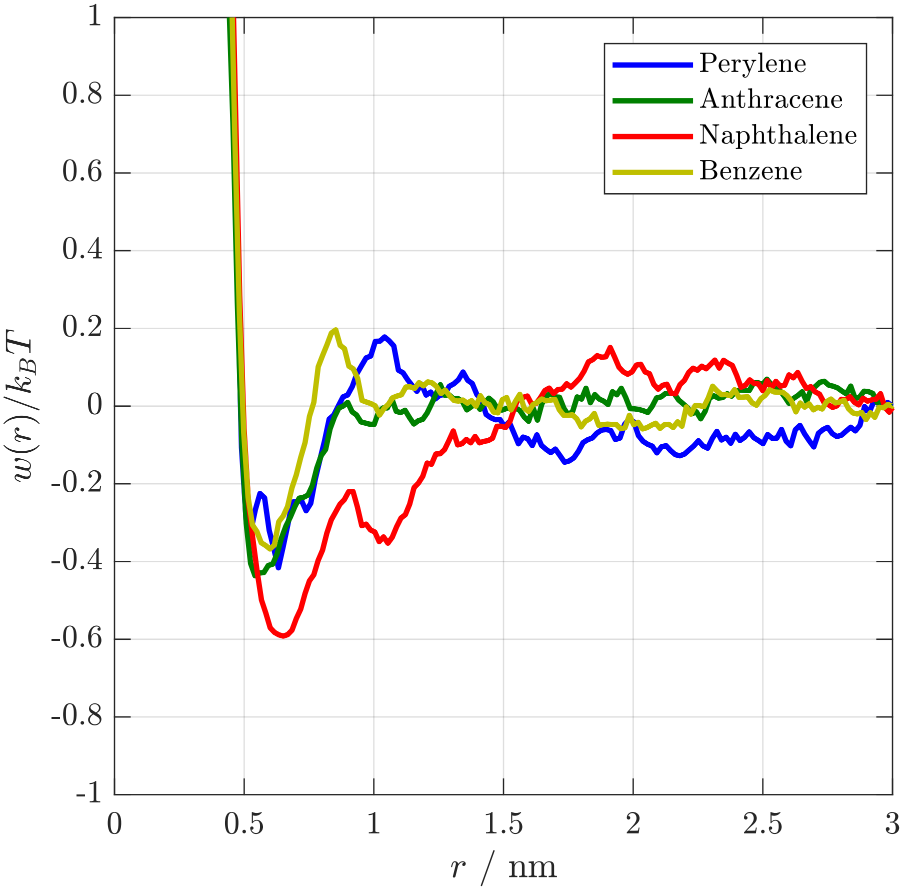

Figure S6: PMF calculations for neutral dimethylaniline and aromatic acceptor pairs in acetonitrile.

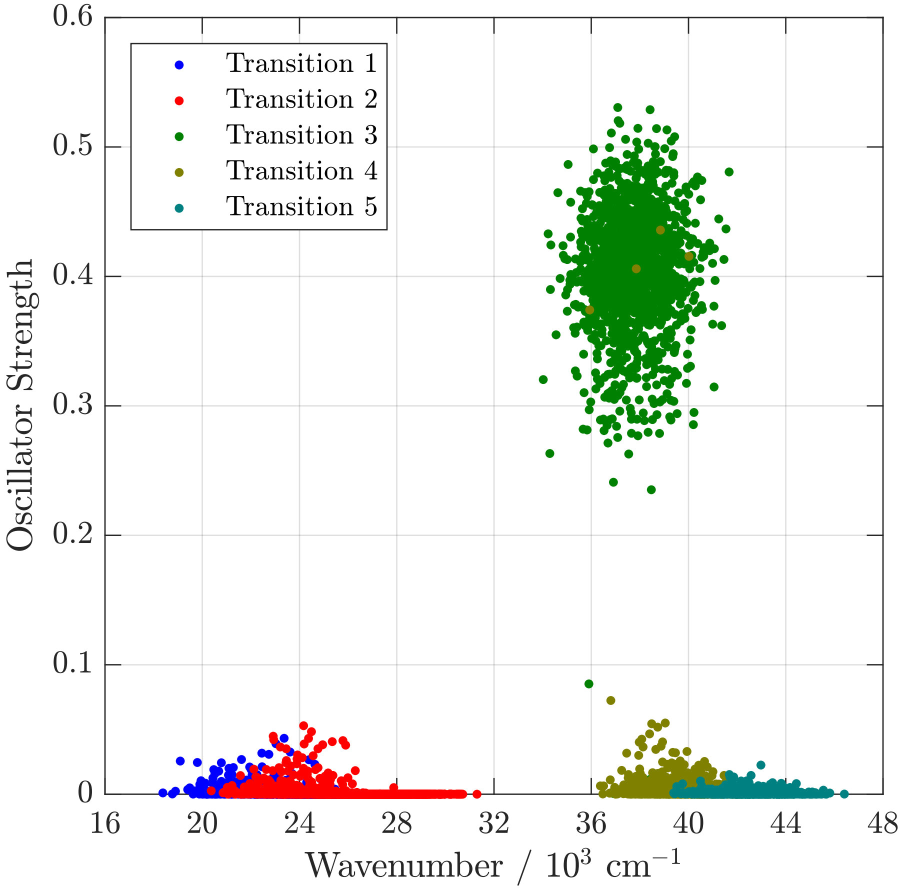

Figure S7: The five lowest energy Bz/TCNE transition oscillator strengths and energies. The lowest 2 transitions involve transitions from Bz HOMOs to the TCNE LUMO and are termed the 'CT transitions', where as the 3 higher energy transitions correspond primarily to local excitation within Bz and TCNE.

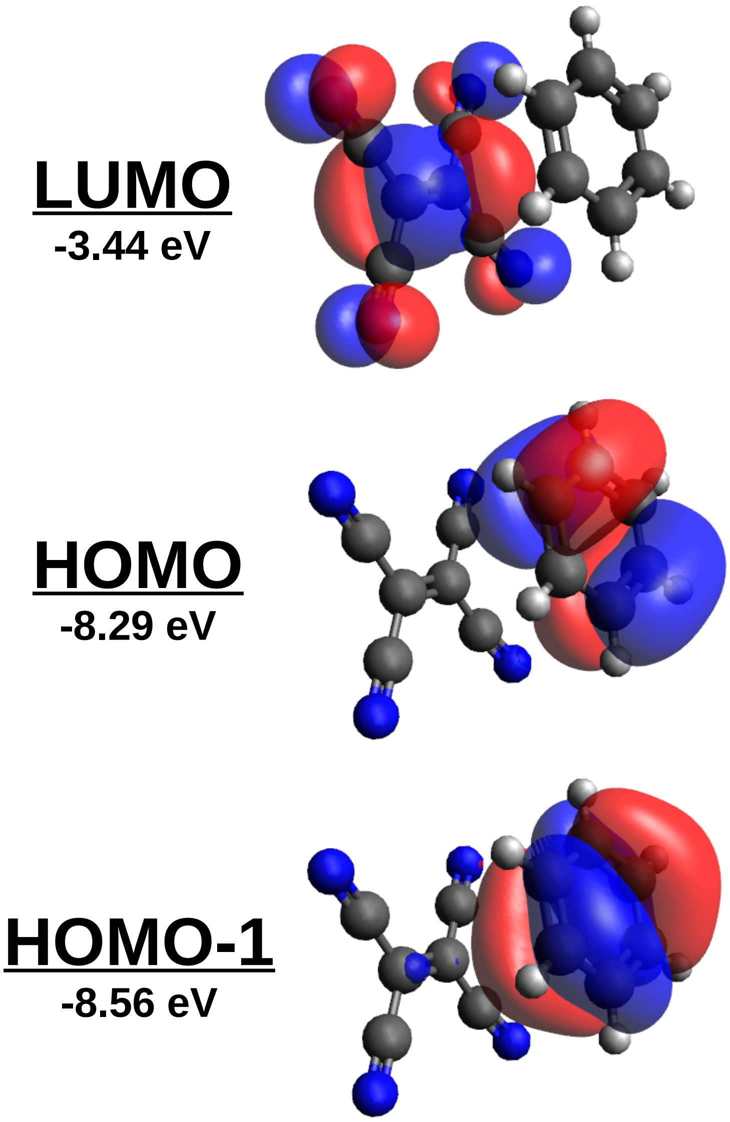

Figure S8: Frontier molecular orbitals involved in Bz/TCNE CT transitions.

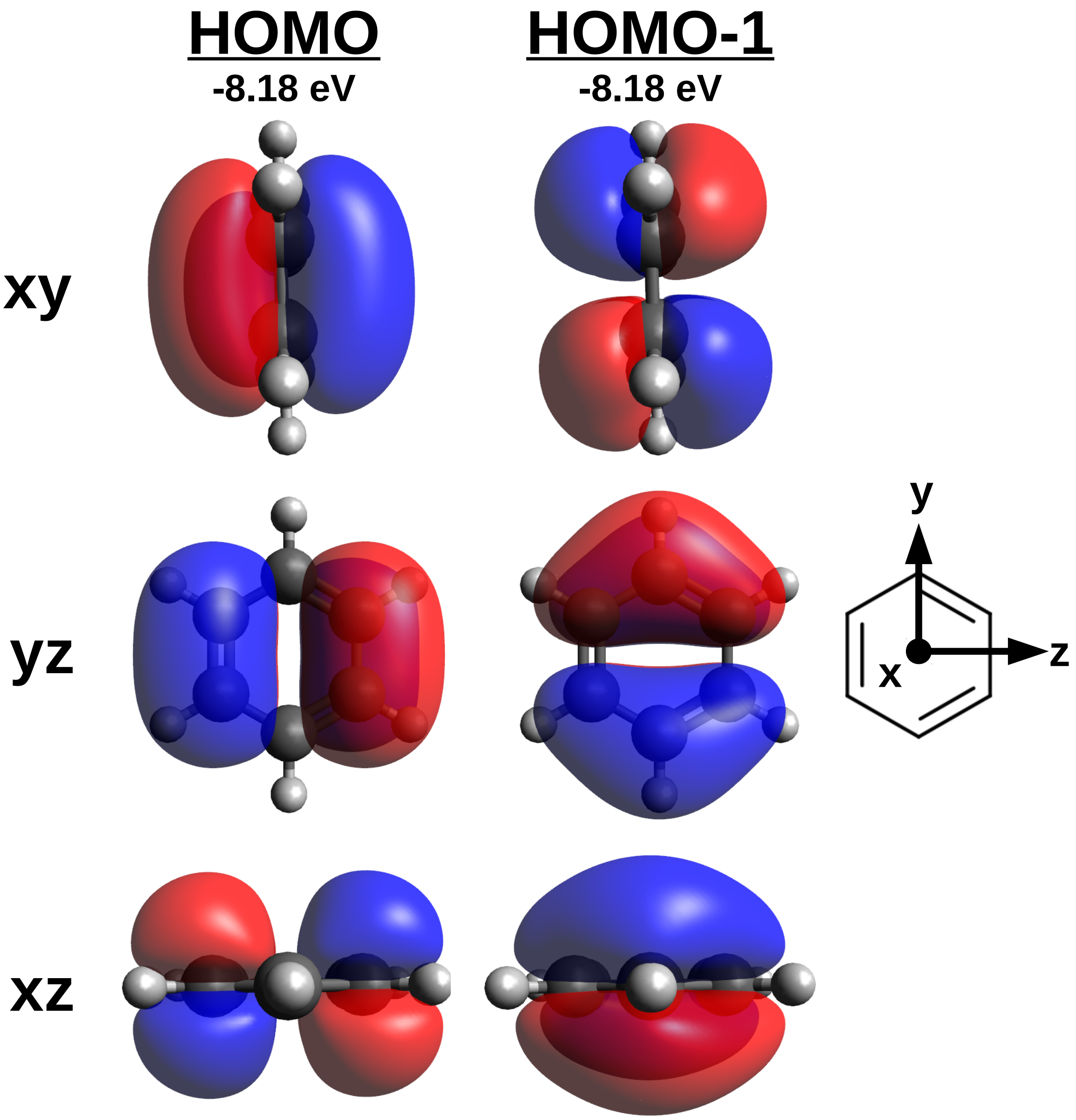

Figure S9: HOMO and HOMO-1 orbitals molecular orbitals of isolated benzene.

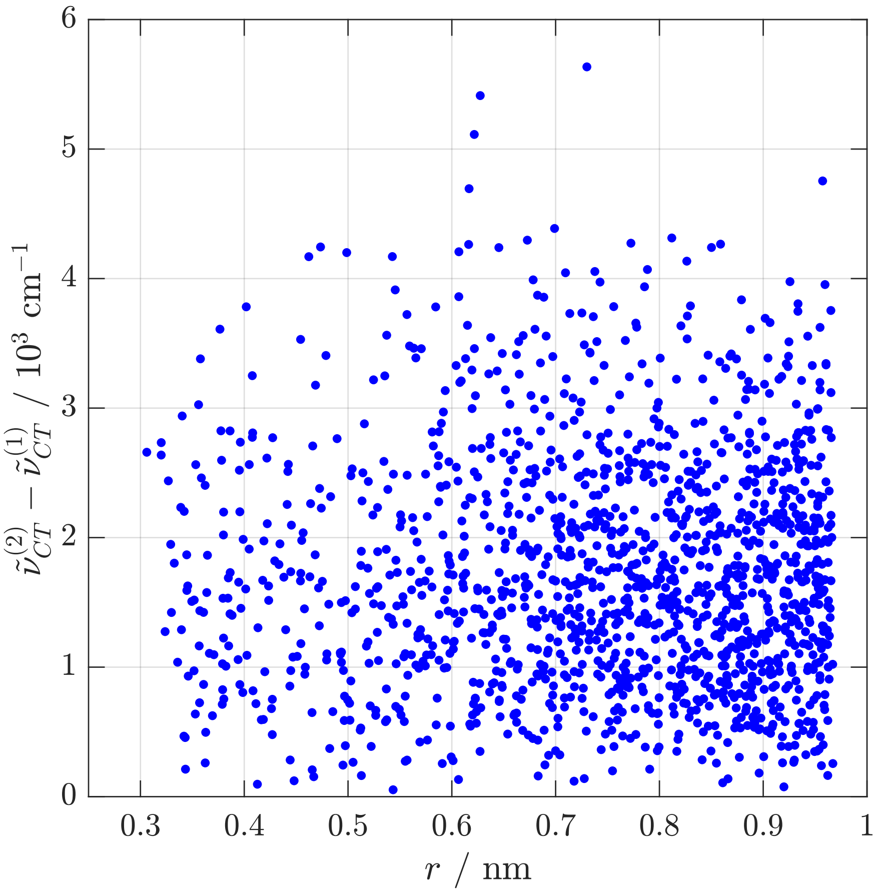

Figure S10: Energy splitting of CT transition frequencies as a function of Bz/TCNE center-of-mass separation.

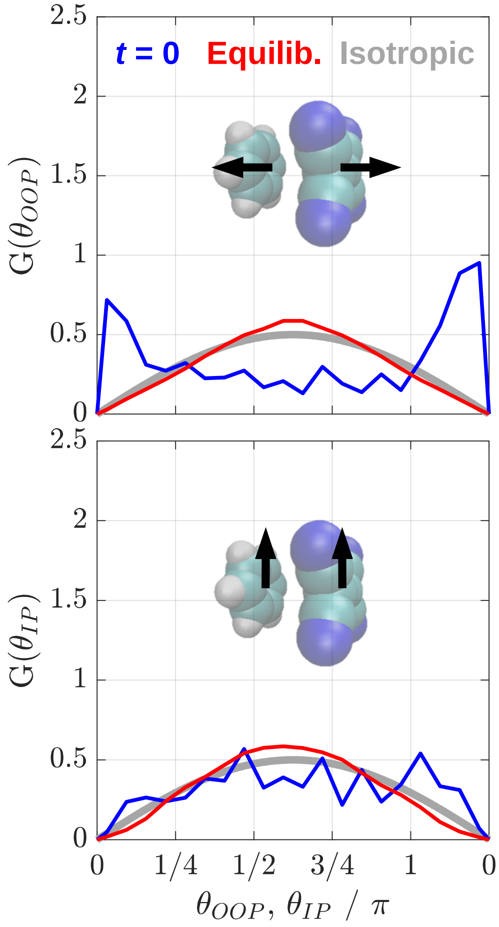

Figure S11: Orientational distributions for Bz and TCNE pairs taken from the non-equilibrium MD simulations. The angles θ_{OOP} and θ_{IP} represent the angles between the out-of-plane and in-plane molecular vectors indicated on each plot and are the same as in Figure 6. These distributions are normalized for unit area. The gray lines represent the expectation for an isotropic distribution of orientations, the blue lines labeled '$t = 0$' represent the initial Bz/TCNE orientations selected from the PMF calculations, and the red lines labeled 'Equilib.' are averages of orientational distributions from 500-1000 ps, times long after the anisotropy has decayed and the system is at conformational equilibrium. An orientation's contribution to the distribution was weighted by the oscillator strength of the initial $t = 0$ pair.

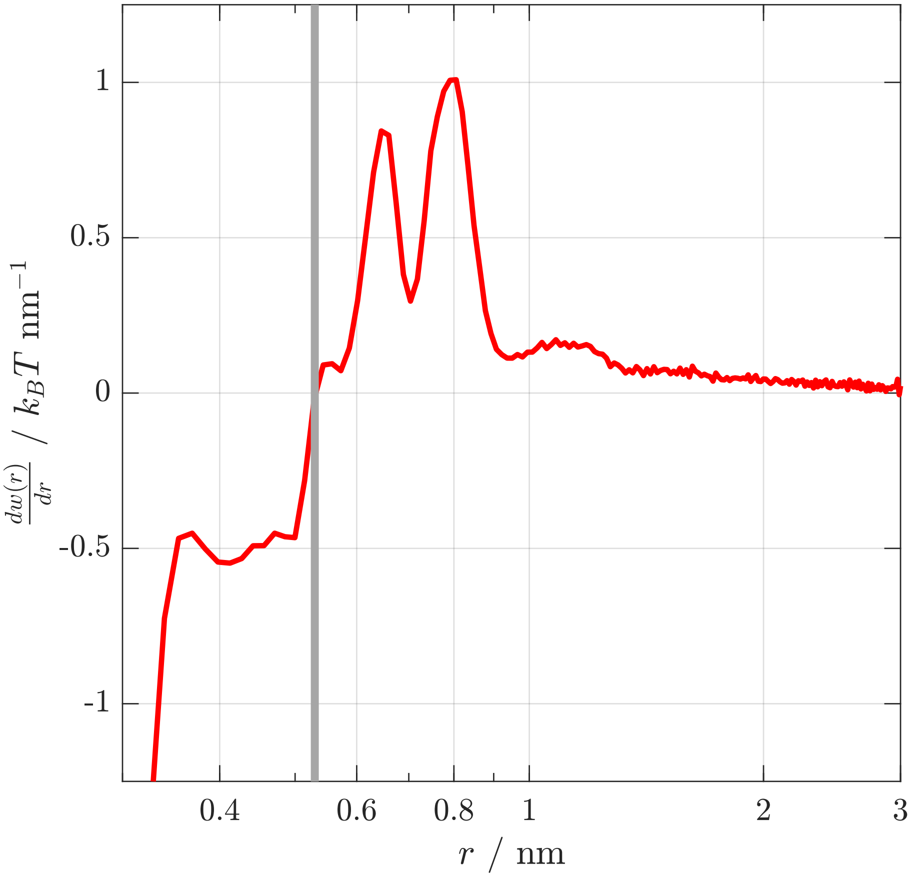

Figure S12: Derivative of the ion pair PMF, $w(r)$ (red curve, Figure 5). The heavy gray line demarcates the minimum of $w(r)$.

References

[1] E. Tokunaga, A. Terasaki and T. Kobayashi, *J. Opt. Soc. Am. B*, 1996, **13**, 496.

[2] I. H. van Stokkum, D. S. Larsen and R. van Grondelle, *Biochim. Biophys. Acta*, 2004, **1657**, 82–104.

[3] J. Bredenbeck and P. Hamm, *Rev. Sci. Instrum.*, 2003, **74**, 3188–3189.

[4] M. J. Abraham, T. Murtola, R. Schulz, S. Páll, J. C. Smith, B. Hess and E. Lindahl, *SoftwareX*, 2015, **1-2**, 19–25.

[5] W. L. Jorgensen, D. S. Maxwell and J. Tirado-Rives, *J. Am. Chem. Soc.*, 1996, **118**, 11225–11236.

[6] U. Essmann, L. Perera, M. L. Berkowitz, T. Darden, H. Lee and L. G. Pedersen, *J. Chem. Phys.*, 1995, **103**, 8577–8593.

[7] B. Hess, *J. Chem. Theory Comput.*, 2008, **4**, 116–122.

[8] G. Bussi, D. Donadio and M. Parrinello, *J. Chem. Phys.*, 2007, **126**, 014101.

[9] N. Michaud-Agrawal, E. J. Denning, T. B. Woolf and O. Beckstein, *J. Comput. Chem.*, 2011, **32**, 2319–2327.

[10] R. J. Gowers, M. Linke, J. Barnoud, T. J. E. Reddy, M. N. Melo, S. L. Seyler, J. Domański, D. L. Dotson, S. Buchoux, I. M. Kenney and O. Beckstein, Proceedings of the 15th Python in Science Conference, 2016, pp. 98–105.

[11] J. S. Hub, B. L. de Groot and D. van der Spoel, *J. Chem. Theory Comput.*, 2010, **6**, 3713–3720.